Available online at www.sciencedirect.com

ScienceDirect

Procedia CIRP 141 (2026) 37–42

www.elsevier.com/locate/procedia

10th Conference on High Performance Cutting (CIRP-HPC 2026)

Geometric simulation of process and tool design for high-speed whirling and high-speed whirl-milling of end mill geometries

Emma Punsmann[a,*], Jannik Schwalm[a], Volker Schulze[a]

[a]*wbk Institute of Production Science, Karlsruhe Institute of Technology (KIT), Kaiserstr. 12, 76131 Karlsruhe, Germany*

* Corresponding author. Tel.: +49-1523-9502596 ; *E-mail address:* emma.punsmann@kit.edu

Abstract

Whirling is widely applied in the manufacturing of threaded components with high surface quality requirements, such as bone screws and precision lead screws. Due to favorable engagement conditions, the process is particularly suitable for hard-to-machine materials like titanium. Synchronized cyclic processes are increasingly used because they offer a high degree of geometric freedom. In synchronized high-speed whirling and high-speed whirl-milling, the rotational speeds of the workpiece and tool are synchronized according to the ratio of thread pitch to the number of cutting edges. This configuration allows for a significant reduction in process time compared to conventional whirling.

This work investigates the geometric feasibility of manufacturing end mill geometries using high-speed whirling and high-speed whirl-milling. Tool and process design for one exemplary end mill variant are derived from geometric penetration calculations and the resulting process parameters for high-speed whirling and high-speed whirl-milling are compared. The simulation results indicate that both processes are fundamentally suitable for producing end mill geometries. Nevertheless, the present work is restricted to a geometric feasibility assessment. Experimental validation is required to evaluate practical applicability, particularly with regard to cutting material selection, achievable surface integrity, and tool wear behavior.

Keywords: Manufacturing process; Geometric modeling; Tool geometry

1. Introduction

Whirling was first patented in 1963 to machine multi-start threads in a single pass [1] and is widely applied to manufacture thread-like components with high surface quality requirements such as bone screws or precision lead screws. In whirling processes the tool rotates at high speed with the cutting tools facing inwards. The pitch of the thread is generated through a slow coupled axial and rotational feed of the workpiece.

In recent years, synchronized cyclic processes have attracted increasing scientific attention. [2] In synchronized high-speed whirling and high-speed whirl-milling, the tool and workpiece axes rotate at synchronous high speeds according to the ratio of thread pitch to the number of cutting edges. This configuration enables a substantial reduction in processing time compared to conventional whirling.

Synchronized high-speed whirling was introduced in 2017 by Klotz et al. to enable its combination with turning operations, resulting in improved cutting conditions and a 30 % increase in productivity. [3] Building on this, high-speed whirl-milling was introduced within the joint research project ”ZykloMed”. In whirl-milling, one or two side-and-face cutters are set at an axis-crossing angle, enabling the production of threads with variable pitch. This process also achieves improved surface quality and increased productivity compared to conventional whirling and further offers enhanced accessibility and chip removal.[4] This work aims to transfer the insights gained in the domain of medical screw manufacturing to the production of end mills (see Figure 1).

In modern CNC and production machining, tungsten carbide has become the predominant material for end mills due to its superior hardness, heat resistance, and rigidity. The conventional manufacturing process for tungsten carbide end mills typically involves green machining prior to sintering, followed by grinding in the fully sintered state. As grinding often represents the most time-consuming step in the production process, research efforts focus on replacing or complementing this process with alternative machining operations, such as milling, in order to reduce both machining time and overall manufacturing costs. [5]

10.1016/j.procir.2026.03.108

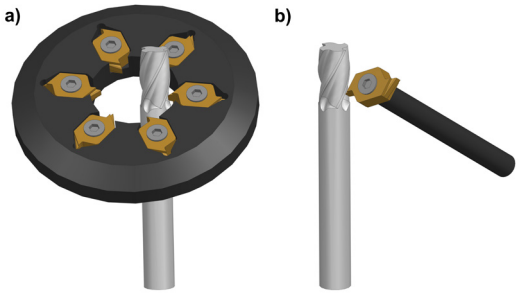

Fig. 1. Process illustration of high-speed whirling a) and high-speed whirl milling b)

However, the machining of hard metals is considered challenging, because of the high hardness leading to accelerated tool wear, comparatively high cutting forces, and poor surface integrity. [6]

Frömming investigated the influence of process parameters for interrupted machining of tungsten carbide with different tool materials. Based on his findings, large negative rake angles are recommended for roughing operations, while small negative rake angles are suggested for finishing in order to minimize subsurface damage. Nevertheless, tool life was extremly limited due to abrasive wear on both rake and flank faces. [6] Ottersbach also showed that weakening of the cutting wedge leads to premature tool failure, but reproducible machining of tungsten carbide was achieved at cutting speeds of $v_c = 70\,\mathrm{m\,min^{-1}}$ with uncut chip thickness $h \leq 15\,\mu\mathrm{m}$ and at $v_c = 140\,\mathrm{m\,min^{-1}}$ with $h \leq 10\,\mu\mathrm{m}$, using a clearance angle of $\alpha = 15°$ and a rake angle of $\gamma = 0°$. While cutting speed had only a minor influence on mechanical loads, it strongly affected thermal loads. [7] Filipović focused on identifying optimal machining parameters for hard metals using CVD-D tools and achieved significant reductions in process time compared to grinding, demonstrating the potential of machining for the production of carbide tools. [5]

These findings suggest that whirling may be particularly suitable for end mill production, as it frequently involves negative rake and small clearance angles, which can be further adjusted through the geometric degrees of freedom inherent to synchronized cyclic processes. Applications in thread manufacturing have already demonstrated the potential of periodic, rotating structures but it remains to be investigated whether these principles can be transferred to end mills, given their steeper helix angles, increased number of threads and the more complex flute geometry. Additionally, synchronized cyclic processes induce strong local variations in process parameters, such as uncut chip thickness, effective normal speed and cutting angles over the tool engagement.

The objective of the present work is therefore a proof-of-concept study, demonstrating the theoretical feasibility of applying high-speed whirling and high-speed whirl-milling to end mill manufacturing and providing initial insights into the resulting cutting conditions with a focus on load distribution along the tool profile and engagement. While this work focuses on theoretical and simulation-based investigations, it provides a basis for experimental validation to assess practical applicability, particularly regarding cutting material selection and achievable surface quality or process design optimized for load distribution and tool life in future studies.

2. Geometric model

The complex process kinematics of synchronized cyclic cutting processes introduce additional degrees of freedom to the process design, as the process depends on both tool design and kinematic configuration. Consequently and since the effective cutting conditions vary significantly along the tool profile and tool–workpiece engagement, extensive design studies and process investigations are required.

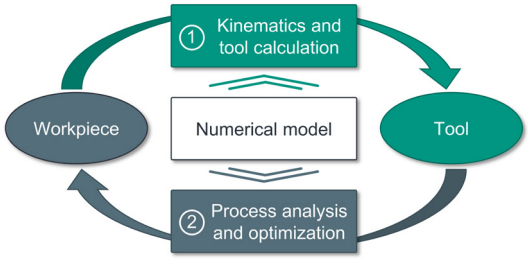

Fig. 2. Geometric simulation workflow

This work builds on an existing simulation framework for synchronized cyclic processes developed at the wbk Institute of Production Science. As established by Hühsam for gear skiving, the process analysis is conducted in two main steps (see Fig. 2). [8] The resulting workpiece geometry is defined by the envelope of the generating motion of the tool profile. Consequently, the cutting-tool geometry cannot be derived from the workpiece contour alone but must incorporate the specific process kinematics. A numerical approach based on spatial and temporal discretization of the targeted workpiece geometry and the machining motion is implemented in the first step. It is based on a dexel-based geometric penetration calculation for determining the cutting tool profile by pointwise trimming of a blank cutting tool in each step by detecting intersections with the surface of the workpiece as first introduced by Zanger et al. [9] After defining the tool geometry, the second step comprises the process analysis and optimization based on parameters such as feed and rotational speeds. The local effective cutting conditions are evaluated through a dexel-based geometric penetration calculation on the uncut chip, following the methodology introduced by Hilligardt et al. In the simulation, the cutting edge is discretized and normal vectors, normal rake face vectors, normal clearance face vectors and local tangential vectors of the cutting edge are defined for every discrete point. The workpiece is modeled by a number of dexel, with triangulated end points. The uncut chip thickness h is calculated along the cutting edge normal on the rake face for every incremental step. Afterwards the workpiece dexel are trimmed against the triangulated sweep surface of the cutting edge in its current position and the step before. The local cutting conditions are derived from the local speed vectors. The resulting effective cutting speed $\vec{v_e}$ corresponds to the relative speed between workpiece and cutting tool

and can be divided into sliding speed $\vec{v_{se}}$, which is tangential to the cutting edge and the effective normal speed $\vec{v_{ne}}$. The effective normal rake and clearance angles, γ_{ne} and α_{ne}, are determined by the relative orientation of the effective normal speed, the local contour normal, and the normal of the clearance face within the cutting edge normal plane. [10]

3. Kinematics and tool calculation

The parameters of the chosen reference geometry are defined according to DIN 6528 [11] and are listed in Table 1. According to the standard, helix angles λ between 30° and 45° are common; hence, the midpoint of this interval was chosen here. Since the shaping of the flutes is not uniquely defined by these parameters, the radius r was introduced. Following the analogy to screw geometry definitions, the rake and clearance faces extend in this radius from the core diameter d_K. Figure 3 shows the workpiece geometry and parameters in cross-section and the 3D extrusion.

Table 1. Reference geometry

Diameter	d_1	8 mm
Number of cutting edges	z	4
Helix angle	λ	37.5°
Rake angle	γ	10°
Clearance angle	α	12°
Core diameter	d_K	5 mm
Radius	r	1 mm

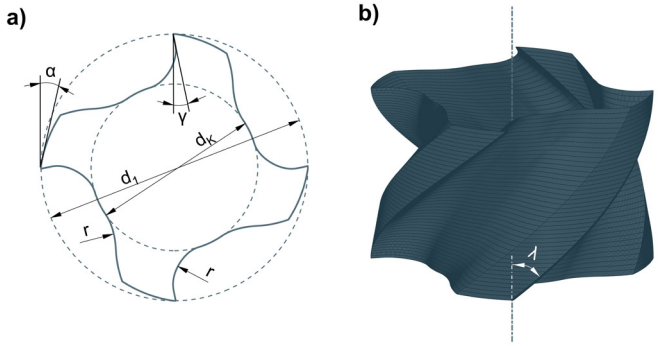

Fig. 3. Workpiece geometry and parameters: cross section a) and 3D-triangulated surface b)

In conventional whirling the tilt angle between the axes of the tool and the workpiece corresponds to the lead angle of the workpiece; for synchronized whirling, this angle corresponds to the vector of relative motion between tool and workpiece. [9] To ensure consistent nomenclature this angle is generally referred to as the axis-crossing Σ in sychronized cyclic processes, which will also be used throughout this work.

As illustrated in Figure 4, high-speed whirling and high-speed whirl-milling differ with respect to the orientation of the cutting edges, which are directed either inwards or outwards. The tool engagement position is determined by the tool outer

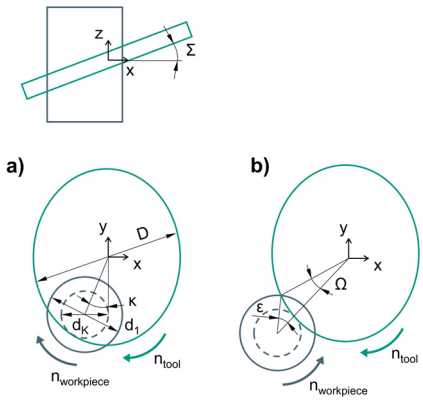

Fig. 4. Process kinematics of high-speed whirling a) and high-speed whirl-milling b)

diameter D and the core diameter of the workpiece d_K. The tool is tilted by the angle Σ about the Y-axis and can additionally be positioned eccentrically by the angle κ. The engagement angles of the tool Ω and the workpiece ε can be derived using the law of cosines. The center distance between tool and workpiece axes is denoted by a. Depending on the configuration, the center distance results in

$$a = \begin{cases} \frac{D}{2} - \frac{d_K}{2}, & \text{whirling} \\ \frac{D}{2} + \frac{d_K}{2}, & \text{whirl-milling} \end{cases} \tag{1}$$

The engagement angles are obtained as

$$\Omega = \arccos\left(\frac{\left(\frac{D}{2} \cdot \cos\delta\right)^2 + a^2 - \left(\frac{d_K}{2}\right)^2}{D \cdot \cos\delta \cdot a} \right) \tag{2}$$

$$\varepsilon = \begin{cases} 180 - \arccos\left(\frac{a^2 + \left(\frac{d_K}{2}\right)^2 - \left(\frac{D}{2} \cdot \cos\delta\right)^2}{a \cdot d_K} \right), & \text{whirling} \\ \arccos\left(\frac{a^2 + \left(\frac{d_K}{2}\right)^2 - \left(\frac{D}{2} \cdot \cos\delta\right)^2}{a \cdot d_K} \right), & \text{whirl-milling} \end{cases} \tag{3}$$

The auxiliary angle δ results from the spatial inclination of the tool axis and is defined as

$$\delta = \arcsin\left(|\sin\Omega| \sin\Sigma\right) \tag{4}$$

For the sake of simplicity, all processes were considered with an eccentricity angle of $\kappa = 0$. Using the formulas presented above, the corresponding engagement angles for the reference workpiece were calculated for various tool diameters and are summarized in Table 2. It can be observed that substantially different engagement angles, and consequently distinct tool–workpiece engagements, occur across the different processes.

Table 2. Engagement angles for high-speed whirling and whirl-milling

D	30 mm	20 mm	15 mm	10 mm
Ω_{whirling}	13.3°	21.3°	30.6°	56.5°
$\varepsilon_{\text{whirling}}$	59.1°	64.1°	70.2°	87.9°
$\Omega_{\text{whirl-milling}}$	11.0°	15.9°	20.5°	29.2°
$\varepsilon_{\text{whirl-milling}}$	45.5°	43.0°	40.8°	36.9°

In high-speed whirling and whirl-milling, multiple threads or flutes are generated by increasing the rotational speed of the workpiece, so that each cutting edge engages a different thread or flute. The rotational speeds of the tool and the workpiece are synchronized according to a whole-numbered ratio, determined by the number of workpiece flutes or cutting edges z and the number of cutting tools Z_T, to avoid damaging the crest or cutting edge of the end mill.

$$n_{\text{workpiece}} = n_{\text{tool}} \cdot \frac{Z_T}{z} \tag{5}$$

As discussed in Section 2 the tool profile depends not only on the chosen workpiece geometry but also on the relative motion during engagement, i.e. process kinematics, tool diameter and number of cutting tools. Based on the reference workpiece geometry from Table 1 and the specifications listed in Table 3, the cutting-edge geometry of the tool is derived using the dexel-based geometric penetration calculation for different numbers of cutting edges. Due to the differing engagement angles, the resulting tool profile for one workpiece geometry varies between high-speed whirling and high-speed whirl-milling. In Figure 5, the tool profiles are superimposed to visualize this effect.

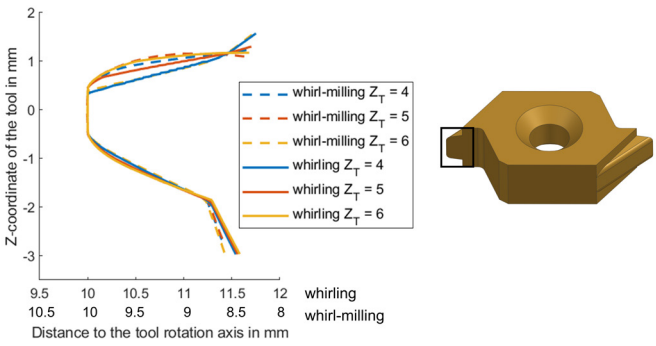

Fig. 5. 2D profile of the cutting edge for different numbers of cutting tools Z_T

It can be observed that, despite identical target workpieces and the same axis-crossing angle, the resulting tool geometries differ in the head region. This variation arises from the differing engagement angles in high-speed whirling and high-speed whirl-milling. Depending on the number of teeth, and consequently the rotation ratio, the upper part of the cutting tool may intersect with the rake face of the workpiece during the trimming process, resulting in a narrower profile that is not initially engaged at the start of cutting. For high-speed whirling, this effect occurs with a reduced number of teeth, whereas for whirl-milling it occurs with an increased number of teeth.

Table 3. Tool and kinematic specifications

Axis-crossing angle	Σ	20°
Eccentricity angle	κ	0°
Tool diameter	D	20 mm

The different process kinematics are also illustrated in Figure 6, where the relative position of the cutting edge to the workpiece gap is shown in 3D (Figure 6a) and b)) and projected into the cross-sectional plane, also referred to as envelope cuts (Figure 6c) and d)). However it can be observed that both processes using either internal or external cutting edges accurately reproduce the workpiece contour.

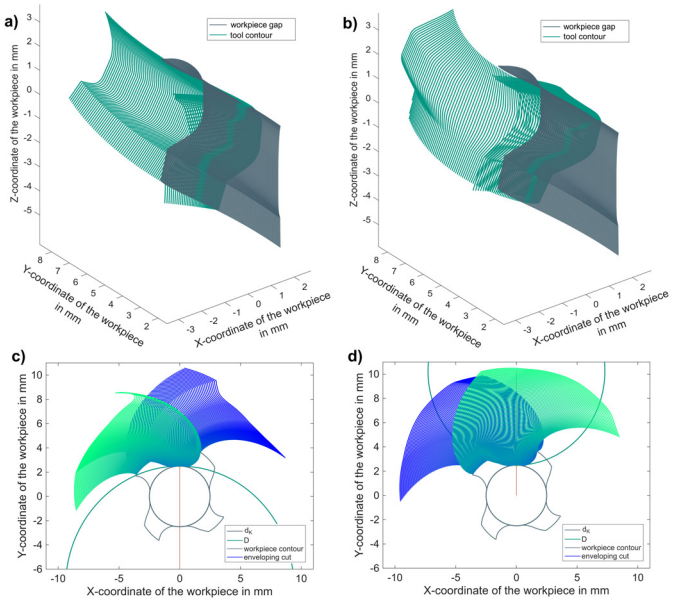

Fig. 6. Relative motion of the cutting edge through the workpiece gap in 3D and projected in the cross-sectional plane for high-speed whirling with $Z_T = 6$ a) and c) and high-speed whirl milling $Z_T = 5$ b) and d)

4. Process simulation and analysis

As is common in other synchronized cyclic processes such as gear skiving, the process is divided into multiple cuts, illustrated in Figure 7, in order to reduce the local uncut chip thickness and improve cutting conditions. For simplicity, a constant radial infeed per cut was assumed, and the number of cuts was determined iteratively until the maximum uncut chip thickness matched the parameter set from Ottersbach described in Section 1. In that study, milling experiments were conducted using

Table 4. Process parameters

Axial feed	s_{ax}	0.02 mm/rev
Cutting speed	v_c	70 m/min
Rotational speed	n_0	1100 rev/min
Number of cuts	c	8
Radial infeed	T	0.1875 mm

a cutting speed of $v_c = 70\,\mathrm{m\,min^{-1}}$ and an uncut chip thickness of $h \leq 15\,\mu\mathrm{m}$. To obtain comparable process parameters in the present work, the rotational speed was calculated based on the cutting diameter of the tool.

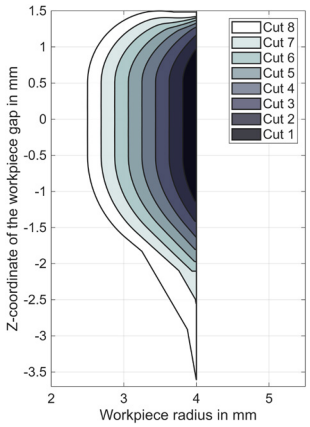

Fig. 7. Axial section of the incremental radial infeed

The local cutting conditions are computed for discrete incremental angular steps and subsequently visualized and evaluated based on characteristic maps. To enable correlation between the maps and the derived cutting-edge geometry, the tool profile is shown in Figure 8a). Figure 8b) depicts the variation of the local uncut chip thickness h over the tool engagement as a function of the tool rotation angle and the Z-coordinate along the tool profile. The resulting shape reflects the tool engagement across the cut and the color gradient represents the variation of the uncut chip thickness. As the tool rotates in the negative angular direction, an increase in uncut chip thickness along the cutting path can be observed. To facilitate the analysis of multiple cuts, the data is condensed by extracting the extreme values at each point along the tool profile. This is illustrated in Figure 8c), where the maximum uncut chip thickness h_{max} at each profile point is plotted along the tool profile.

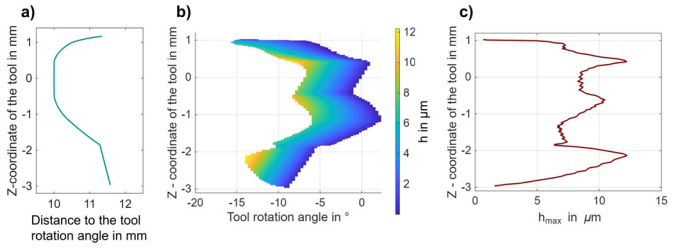

Fig. 8. Tool profile a) and characteristic map of the maximum uncut chip thickness h in the last cut b) and maximum chip thickness c) for high-speed whirling with $Z_T = 6$

The influence of the varying tool profiles, resulting from changes in the number of cutting tools, can be observed in Figures 9 and 10. It can be seen that the different tool profiles lead to distinct characteristic maps. The profiles with reduced head geometries cause a shift and a local increase in the uncut chip thickness at the initial point of engagement. It can also be noted that the tool engagement differs between the two processes, which can be attributed to the distinct process kinematics illustrated in Figure 6. Overall, however, the distributions are comparable in magnitude and general trend.

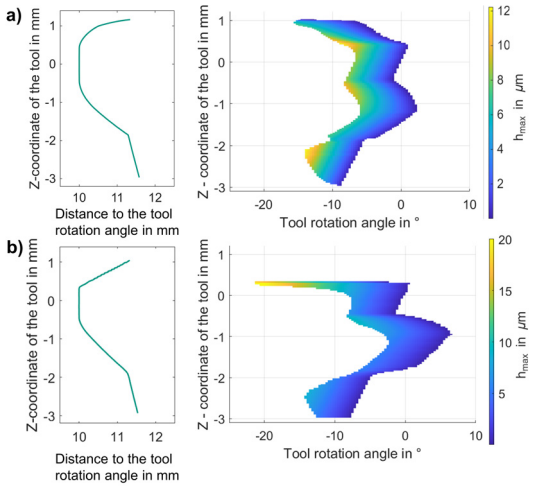

Fig. 9. Tool profile and characteristic map of the maximum uncut chip thickness h in the last cut for high-speed whirling with with $Z_T = 6$ a) and with $Z_T = 4$ b)

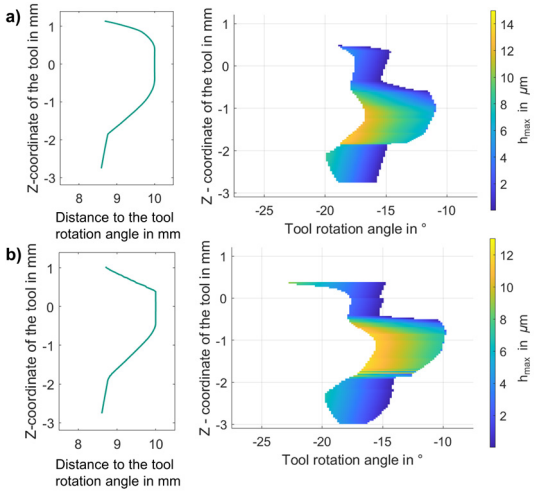

Fig. 10. Tool profile and characteristic map of the maximum uncut chip thickness h in the last cut for high-speed whirling with with $Z_T = 4$ a) and with $Z_T = 6$ b)

Figure 11a) and b) show the maximum local uncut chip thickness h_{max} over all cuts. In high-speed whirling the maximum uncut chip thickness generally decreases with successive cuts, whereas in high-speed whirl-milling it gradually increases. For both processes, the lower section of the cutting edge responsible for generating the clearance face only becomes active during the final cuts. The maximum nominal un-

cut chip thickness remains below 15 µm for both processes and therefore within the defined operating window.

An examination of the results in Figure 11c) and d) reveals that the evolution of the effective normal cutting speed $v_{ne\ max}$ is relatively similar across all cuts within one process. However, the dispersion of the normal cutting speed is more pronounced in high-speed whirl-milling, which can be attributed to the orientation of the cutting edges: in high-speed whirling the lower section of the cutting edge is located at a larger diameter, whereas in high-speed whirl-milling it is situated at a smaller diameter, leading to lower effective speeds in general.

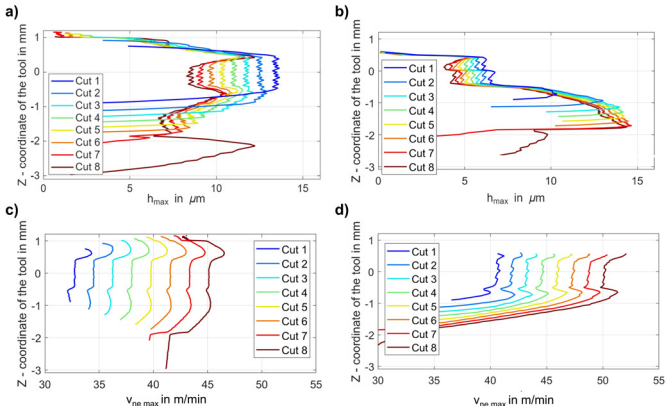

Fig. 11. Maximum uncut chip thickness h_{max} over all cuts for high-speed whirling a) and high-speed whirl milling b) and maximum effective normal speed $v_{ne\ max}$ over all cuts for high-speed whirling c) and high-speed whirl-milling d)

To assess the load acting on the cutting edge, the load equivalent V'_e, as introduced by Hilligardt and Schulze, is employed in Figure 12. It is defined as the integral of the product of the effective normal cutting speed v_{ne} and the uncut chip thickness h over one cut [12]. As discussed above, the lower part of the cutting edge, which is responsible for generating the clearance face of the workpiece, is subjected to comparatively low loading. Due to the increased normal speed in high-speed whirl-milling the sum of the load equivalent V'_e is higher compared to high-speed whirling. Based on findings from gear skiving processes, elevated tool wear is to be expected in this area of the cutting edge.

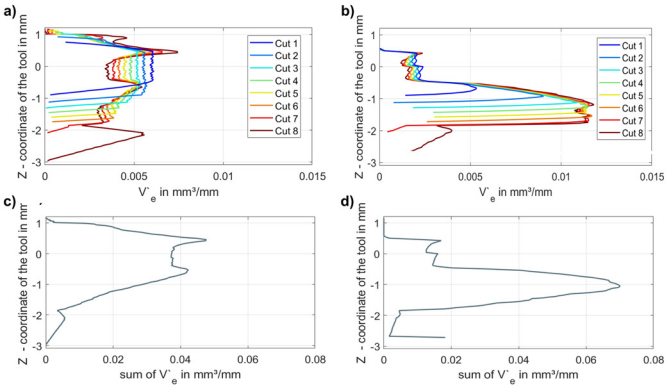

Fig. 12. Load equivalent $V'e$ for each cut and the sum for high-speed whirling a) and c) and high-speed whirl milling b) and d)

5. Conclusion

This work demonstrated that synchronized high-speed whirling and high-speed whirl-milling are fundamentally suitable for the manufacturing of end mill geometries. The tool and process design were carried out for an exemplary end mill configuration, highlighting the influence of rotation ratios on the resulting tool profiles in both processes. Based on this design, the local effective cutting conditions were determined for a defined reference process. The results indicate that, by applying multiple cuts and small axial feed rates, both processes can in principle be operated within the established process window for tungsten carbide machining. For the investigated reference case, high-speed whirling appears slightly more favorable due to a more uniform distribution of cutting-edge load.

However, as with other synchronized cyclic and kinematically complex processes, additional degrees of freedom exist whose potential was not fully exploited in this initial proof-of-concept study. Future work should therefore focus on systematic process optimization and experimental validation. Beyond validating the geometric feasibility and analyzing potential deviations, further investigations must address the selection of suitable cutting tool materials and examine the achievable surface integrity.

References

[1] K. Burgsmüller, Verfahren zum Wirbeln von Gewinden und Vorrichtung dazu, Patent DE1234567 (1963).
[2] V. Schulze, T. Arndt, Effiziente Zerspanung: Synchronisiert zyklische Verfahren für hohe Produktivität und neue geometrische Freiheiten, Moderne Zerspanungstechnologie: Neue Entwicklungen und Trends aus Forschung und Praxis (2024) 1–11.
[3] S. Klotz, F. Zanger, V. Sellmeier, V. Schulze, Signifikant leistungsfähiger – synchroner Drehwirbel-Prozess, WB Werkstatt + Betrieb 12/2016 (2016) 62–65.
[4] T. Arndt, V. Schulze, Funktionsintegrierte Implantate durch neuartige synchronisiert-zyklische Zerspanung Zyklomed (2024).
[5] L. Filipović, Fräsbearbeitung von Wolframcarbid-Kobalt-Hartmetall mit CVD-D-Diamantwerkzeugen, Ph.D. thesis, Technische Universität Wien, Wien (2022).
[6] H. Frömming, Zerspanung von WC-Co-Hartmetall im unterbrochenen Schnitt, Ph.D. thesis, Technische Universität Hamburg (TUHH), Hamburg (2011).
[7] M. Ottersbach, Belastungsspezifische Werkzeug- und Prozessauslegung für die Schlichtfräsbearbeitung von Hartmetall, Ph.D. thesis, RWTH Aachen University, Aachen (2018).
[8] A. Hühsam, Modellbildung und experimentelle Untersuchung des Wälzschälprozesses, Ph.D. thesis, Karlsruher Institut für Technologie (KIT), Karlsruhe (2002).
[9] F. Zanger, V. Sellmeier, J. Klose, M. Bartkowiak, V. Schulze, Comparison of modeling methods to determine cutting tool profile for conventional and synchronized whirling, Procedia CIRP 58 (2017) 222–227.
[10] A. Hilligardt, F. Böhland, J. Klose, M. Gerstenmeyer, V. Schulze, A new approach for local cutting force modeling enabling the transfer between different milling conditions and tool geometries, Procedia CIRP 102 (2021) 138–143.
[11] Deutsches Institut für Normung, DIN 6528: Vollhartmetall-Schaftfräser mit durchgehendem Zylinderschaft – Maße (2002).
[12] A. Hilligardt, V. Schulze, A holistic approach for gear skiving design enabling tool load homogenization, CIRP Annals 71 (2022) 85–88.